

### Contents lists available at ScienceDirect

### Energy

journal homepage: www.elsevier.com/locate/energy



# Exergy analysis and parametric optimization of three power and fresh water cogeneration systems using refrigeration chillers



### I. Janghorban Esfahani, C.K. Yoo\*

Dept. of Environmental Science and Engineering, College of Engineering, Center for Environmental Studies, Kyung Hee University, Seocheon-dong 1, Giheung-gu, Yongin-Si, Gyeonggi-Do 446-701, Republic of Korea

### ARTICLE INFO

Article history:
Received 12 January 2013
Received in revised form
13 May 2013
Accepted 21 July 2013
Available online 15 August 2013

Keywords:
Cogeneration
Exergy
GT (gas turbine)
Optimization
RO (reverse osmosis)

### ABSTRACT

Three power and fresh water cogeneration systems that combine a GT (gas turbine) power plant and a RO (reverse osmosis) desalination system were compared based on the exergy viewpoint. In the first system, the GT and RO systems were coupled mechanically to form a base system. In the second and third systems, a VCR (vapor-compression refrigeration) cycle and a single-effect AC<sub>Water-LiBr</sub> (water/lithium bromide absorption chiller) were used, respectively, to cool the compressor inlet air and preheat the RO intake seawater via waste heat recovery in the VCR condenser and AC<sub>Water-LiBr</sub> absorber. A parametric analysis-based exergy was conducted to evaluate the effects of the key thermodynamic parameters including the compressor inlet air temperature and the fuel-mass flow rate on the system exergy efficiency. Parameter optimization was achieved using a GA (genetic algorithm) to reach the maximum exergy efficiency, where the thermodynamic improvement potentials of the systems were identified. The optimum values of performance for the three cogeneration systems were compared under the same conditions. The results showed that the cogeneration system with the AC is the best system among the three systems, since it can increase exergy and energy efficiencies as well as net power generation by 3.79%, 4.21%, and 38%, respectively, compared to the base system.

 $\ensuremath{\text{@}}$  2013 Elsevier Ltd. All rights reserved.

### 1. Introduction

Power and fresh water are two important requirements that are simultaneously needed in many regions, climates, and industries. Water is available in large quantities on earth, but only a small amount is low enough in salinity for drinking and irrigation. Desalination of sea and brackish water is the main source of fresh water in regions suffering from scarcities of natural fresh water supplies [1,2]. The two most widely used desalination techniques are RO (reverse osmosis) membrane separation and thermal desalination systems, such as MED (multi-effect distillation) and MSF (multi-stage flash) [3,4]. The energy consumption of the RO desalination systems is less than thermal desalination systems which is only in the form of shaft work (electric power). GT (Gas turbine) and steam turbine power plants are widely utilized throughout the world for electricity generation. Design and construction of the GT power plants are simpler than those of the steam turbine and more useful in regions facing water scarcity.

Therefore, coupling the GT power plants and the RO systems is known to be the simplest way to generate the power and fresh water, simultaneously [5,6].

In hot climates, the efficiency and power output of GTs can be enhanced by reducing the compressor inlet air temperature [7]. Different methods are used to cool the intake air of the GT compressor. These include evaporative coolers, spray inlet coolers or fogging systems, and mechanical vapor compression or ACs (absorption chillers) [8]. Evaporative coolers require a dematerialized water supply while compression and ACs use shaft work and heat as the energy input, respectively [7]. Therefore, compression chillers can be mechanically coupled to the GT by shaft and ACs can be thermally coupled to the GT power plant via waste heat recovery from the GT exhaust gases using a HRSG (heat recovery steam generator).

Recently, several studies [7–16] have been performed on utilizing evaporative cooling, mechanical vapor compression, and ACs to cool the compressor inlet air in the GT power plants. Popli et al. [7] investigated using the single-effect AC<sub>Water-LiBr</sub> (water/lithium bromide AC) for cooling the inlet air of the GT compressor, with particular applicability to Middle East countries. Khaliq and Dincer [12] applied exergy method to analyze the GT cycle cogeneration

<sup>\*</sup> Corresponding author. Tel.: +82 31 201 3824; fax: +82 31 202 8854. E-mail address: ckyoo@khu.ac.kr (C.K. Yoo).

with inlet air cooling and evaporative aftercooling of compressor discharge. They reported that the inlet air cooling along with evaporative aftercooling has an obvious increase in the energy and exergy efficiency.

In compression and ACs, to continue the refrigeration cycle, the heat should be transferred to the environment, which can be recovered for many purposes. In the RO desalination systems, for constant fresh water production, the power consumption decreases with increase in feed water temperature. Because, increase in feed water temperature decreases both the osmotic pressure differential across the membrane and water viscosity [17]. Therefore, the waste heat of the refrigeration chillers can be recovered to preheat the RO feed water which lead to improve the RO performance.

A few studies [5,8] has recently been performed on preheating the RO feed water via waste heat recovery from other processes. Ataei et al. [5] investigated the effect of the preheating the seawater through the waste heat recovery from the VCR (vapor-compression refrigeration) cycle on the RO power consumption. Janghorban Esfahani et al. [8] proposed a new combined GT and RO desalination systems which uses a VCR system to cool the compressor inlet air and to preheat the RO feed water by waste heat recovery from the refrigeration system condenser.

According to the literature review, only the use of compression refrigeration chillers has been investigated in combined GT power plant and RO desalination systems. However, the use of ACs in combined GT and RO systems is scare.

Since GT power plants, refrigeration cycles, and RO desalination systems are energy-intensive industries, energy analysis is used to assess and improve their performance. In addition, exergy analysis needs to be used because energy analysis gives no information on how, where, and how much the system performance is degraded [18]. Exergy analysis usually aims to determine the maximum performance of the system and identify the equipment in which exergy loss occurs, and indicate the possibilities for thermodynamic improvement of the system [19].

Several studies have conducted exergy analysis for GTs, refrigeration, and RO desalination systems [18–37]. Dai et al. [22] performed an exergy analysis to guide thermodynamic improvement

for a new combined power and refrigeration cycle. Gebreslassie et al. [23] performed an exergy analysis for single-, double-, triple-, and half-effect Water/Lithium bromide absorption cycles. They also determined the exergy efficiencies and exergy destruction rates for each system. As were investigated in the literature, recent research efforts have been focused on an exergy analysis of cogeneration systems but few studies on the exergy analysis of the combined power and fresh water systems integrated with refrigeration systems are scarce.

This study contributes to propose a new combined GT and RO desalination system which couples the GT and RO systems mechanically via the shaft of the GT and thermally via the AC. In the proposed structure the waste heat of the GT exhaust gases is recovered to generate steam as an energy source for the single-effect  $H_2O/LiBr$  absorption chiller ( $AC_{H_2O-LiBr}$ ) system. The inlet air of the GT compressor is cooled using the evaporator, and the waste heat of the absorber is utilized to preheat the feed water of the RO system to decrease the power consumption of the combined system as a contribution of research. Also it is compared to two other combined GT and RO systems from the viewpoint of exergy to evaluate the capability value of the suggested system to increase the exergy efficiency than those of the two other systems.

This paper consists of three major parts. First, a thermodynamic model is developed to simulate and specify the thermodynamic properties of the systems. Second, exergy analysis is conducted to determine the exergy destruction in the components and exergy efficiencies of the systems. Also the effects of the two key parameters of the compressor inlet air temperature and the fuel-mass flow rate on the exergy efficiencies are investigated. Third, the optimal operating values of the parameters for maximizing exergy efficiency are obtained by using a GA (genetic algorithm), which can identify the thermodynamic improvement potentials of the systems.

### 2. Materials and methods

### 2.1. System configurations

The three systems under consideration are shown in Figs. 1–3. The base system (GT–RO system, Fig. 1) comprises two subsystems:

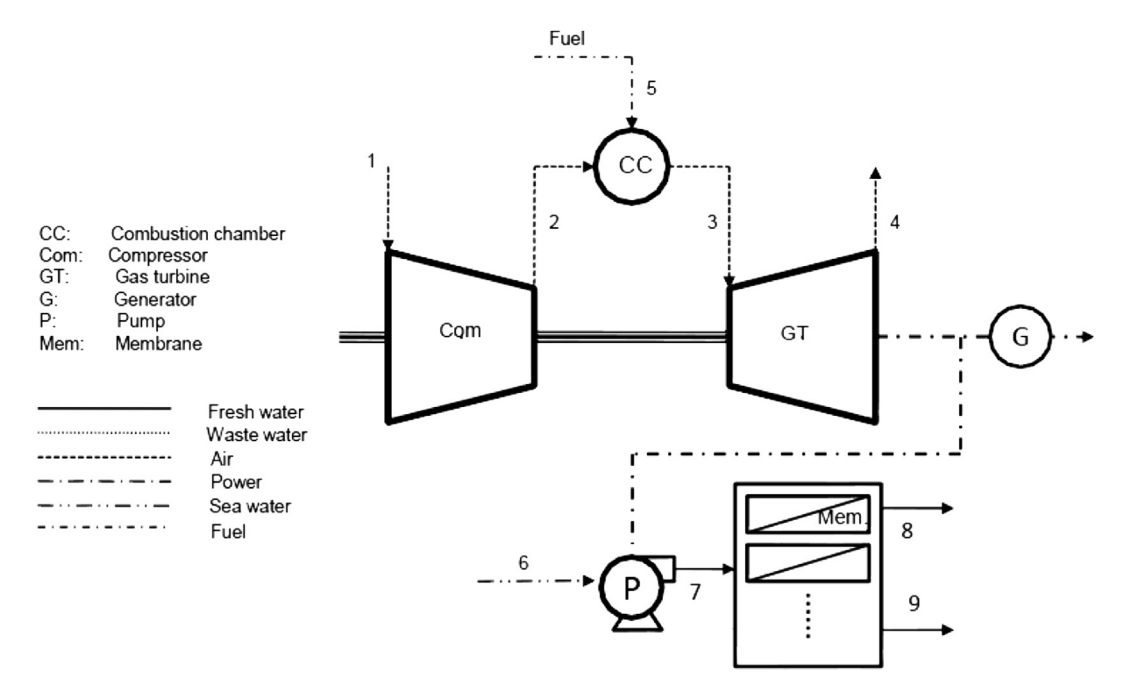


Fig. 1. Schematic of GT-RO system (first system) [6].

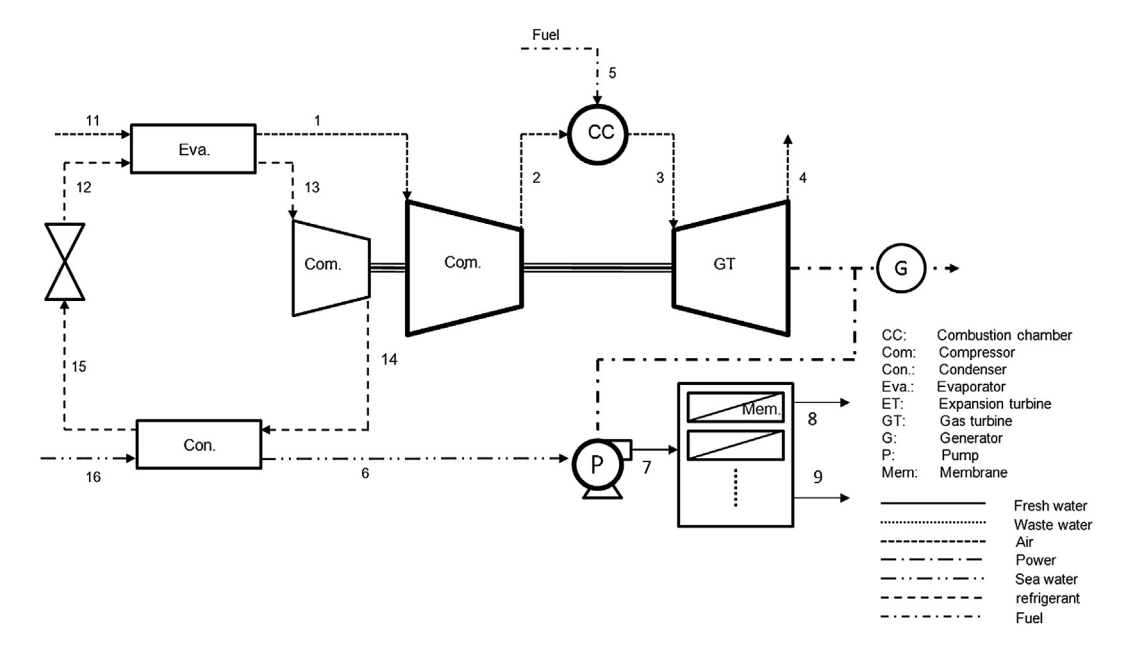
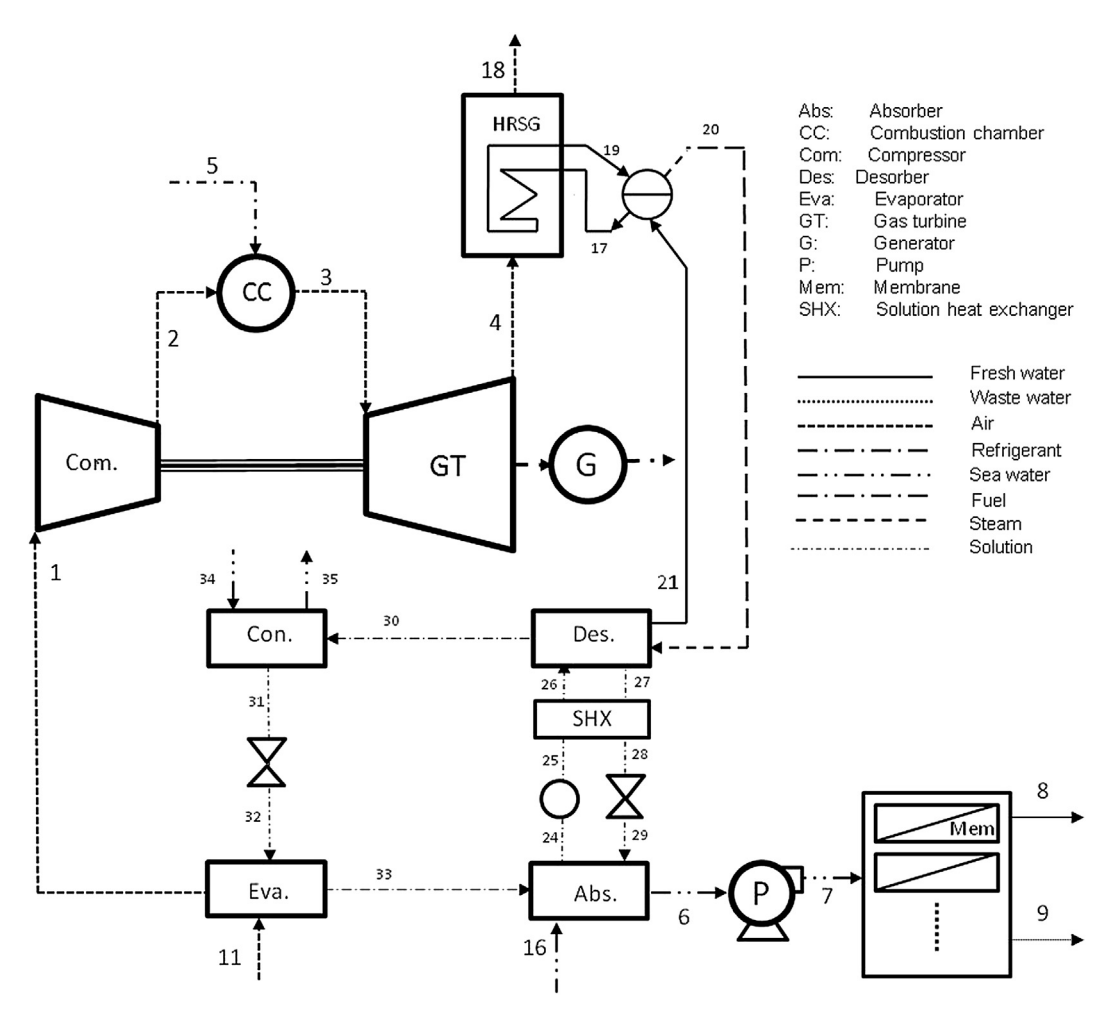


Fig. 2. Schematic of GT-VCR-RO cogeneration system (second system) [8].



**Fig. 3.** Schematic of a new GT–ARC–RO cogeneration system (third system).

a GT power plant and a RO desalination system, which are coupled together mechanically. In the GT subsystem, the air at ambient temperature is compressed using an air compressor and then sent to a CC (combustion chamber) where the fuel is injected. The hot gas is expanded through the GT and shaft work is generated to operate the generator and the pump of the RO system. Expanded gas is discharged to the atmosphere through a stack. In the RO subsystem, the seawater is pumped into the membranes, which are inserted in cylindrical pressure vessels. The water molecules pass through the membrane which increases the concentration of the rejected water and produce fresh water on the other side.

Note that the power generation and efficiency of the system in the GT subsystem increases by decrease in compressor inlet air temperature, and the power consumption of the RO pump in the RO subsystem decreases by increasing the feed water temperature, since it reduce (the osmotic pressure differential across the membrane and water viscosity). A refrigeration system is used in Figs. 2 and 3 for dual purposes: first, decreasing the compressor inlet air temperature of the GT subsystem using the evaporator of the refrigeration system, and second, increasing the feed water temperature of the RO subsystem by waste heat recovery from the condenser of the refrigeration system. Therefore, using a refrigeration system between compressor inlet air and RO feed water streams in both systems presented in Figs. 2 and 3 improves the performance of the combined system by cooling the compressor inlet air and heating the RO feed water, simultaneously.

In the system presented in Fig. 2 as the second system (GT–VCR–RO system), a VCR system is used as the refrigeration system. In the GT–VCR–RO system, the air is cooled by the evaporator of the VCR system and then compressed by the air compressor. The compressed air with injected fuel is sent to the CC. The hot gas is expanded in the GT where the shaft work is generated. The generated shaft work is applied to operate the generator, the RO pump, and the VCR system's compressor. The waste heat from the condenser of the VCR system is recovered to increase the RO feed water temperature. Preheated feed water is then passed through the RO membranes at a high pressure provided by the RO pump, and the brine stream at a high pressure is rejected back to the sea.

In the system presented in Fig. 3 as the third system  $(GT-AC_{H_2O-LiBr}-RO\ system)$ , a single-effect  $(AC_{H_2O-LiBr})$  is used as the refrigeration system. The compressor inlet air temperature is decreased by the evaporator of the  $AC_{H_2O-LiBr}$  system and then compressed by the compressor of the GT. The compressed air with injected fuel is sent to the GT. The hot gas is expanded in the GT, and the shaft work is generated to operate the generator, the GT0 pump, and the GT1 system's pump. The heat of the GT2 outlet gasses is recovered using a HRSG to generate saturated steam as a heat source for the desorber of the GT3 system is recovered to increase the GT4 feed water temperature. Preheated feed water is pumped by a high pressure pump and passed through the GT4 membranes. The brine is rejected back to the sea at a high pressure and the fresh water is produced in the other side of the membranes.

### 2.2. Thermodynamic model of the combined GT and RO systems

In order to conduct energy and exergy analysis of the three cogeneration systems, the thermodynamic properties of the systems must be specified. This is usually done through thermodynamic modeling. This section includes the equations of the thermodynamic model of the cogeneration systems. The major portion of this model consists of the mass, salinity, and energy balance equations. The models developed by Janghorban Esfahani et al. [8], Ahmadi and Dincer [20], Marcovecchio et al. [38], Vince et al. [39], and Hosseini et al. [40] have been used in this study.

Several simplifying assumptions in the development of thermodynamic model are listed below:

- The cogeneration systems are operated under steady state conditions.
- Heat losses and pressure drops in piping and the components are negligible.
- The water/lithium bromide concentrations are zero in steam phase.
- The water/lithium bromide solution in the desorber and absorber outlet is saturated.
- The refrigerant in the evaporator and condenser outlet of VCR cycle is saturated.

Each system has been modeled as three subsystems, as described below.

### 2.2.1. GT power plant subsystem

Fig. 4 shows the temperature—entropy (T-s) diagram of the real open GT cycle. Three irreversible processes including non-isentropic compression (line 1–2), non-isobaric heat addition (line 2–3), and non-isentropic expansion (line 3–4) processes which are deviated from the ideal process due to the irreversibilities, are modeled by Eqs. (1)–(10).

2.2.1.1. AC (air compressor). As shown in Fig. 4, the actual outlet temperature of the air compressor  $(T_2)$  is more than the ideal outlet temperature of the air compressor  $(T_{2i})$  due to irreversibility during the compression process. The outlet air temperature of the air compressor with isentropic efficiency of  $\eta_{\text{com,cr}}$  is given by Eq. (1) [12].

$$T_2 = T_1 \times \left(1 + \frac{1}{\eta_{\text{com.cr}}} \left(r_{\text{com.cr}}^{\frac{\gamma_a - 1}{\gamma_a}} - 1\right)\right) \tag{1}$$

where  $T_1$ ,  $T_2$ ,  $\eta_{\text{com.}_{\text{CT}}}$  and  $r_{\text{com.}_{\text{CT}}}$  are the inlet air temperature, outlet air temperature, isentropic efficiency, the pressure ratio of the air compressor, respectively, and  $\gamma_a$  is the heat capacity ratio of air. The power consumption of the air compressor is given by Eq. (2) [41].

$$\dot{W}_{\text{com.gr}} = \dot{m}_a \left( C_{\text{pa}(T_2)} T_2 - C_{\text{pa}(T_1)} T_1 \right)$$
 (2)

where  $\dot{W}_{\text{com.}_{\text{CT}}}$  is the power consumption of the air compressor,  $\dot{m}_a$  is air mass flow rate.  $C_{\text{pa}(T_1)}$  and  $C_{\text{pa}(T_2)}$  are the specific heat of air at  $T_1$  and  $T_2$  which can be calculated by Eq. (3) [42].

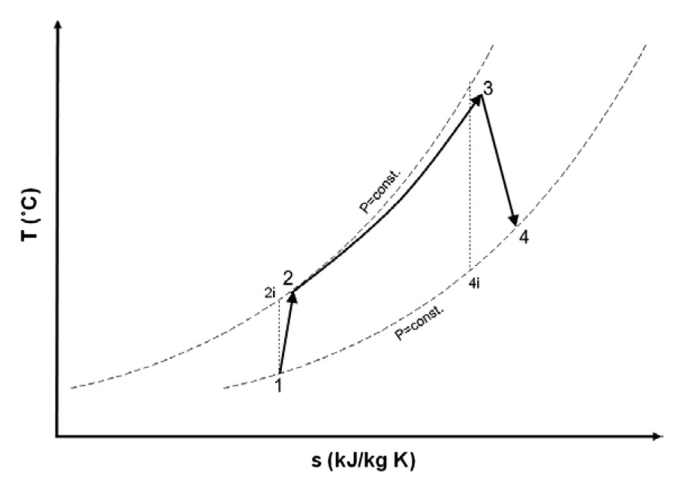


**Fig. 4.** Temperature—entropy (*T*–*s*) diagram of the GT cycle.

$$\begin{split} C_{pa(T)} \, = \, 1.04841 - \left( \frac{3.8371T}{10^4} \right) + \left( \frac{9.4537T^2}{10^7} \right) - \left( \frac{5.49031T^3}{10^{10}} \right) \\ + \left( \frac{7.9298T^4}{10^{14}} \right) \end{split}$$

(3)

where  $C_{pa(T)}$  is the specific heat of air at temperature of T.

*2.2.1.2. CC.* The energy balance equation of the CC is given by Eq. (4) [43].

$$\dot{m}_{\text{fuel}}\eta_{\text{cc}}\text{LHV} = \dot{m}_g \cdot C_{\text{pg}(T_3)}T_3 - \dot{m}_a C_{\text{pa}(T_2)}T_2 \tag{4}$$

where  $\dot{m}_{\rm fuel}$ ,  $\dot{m}_{\rm g}$ , and  $\dot{m}_a$  are fuel, gas and air mass flow rates,  $\eta_{\rm cc}$  is the CC heat efficiency, LHV is the low heat value of fuel,  $C_{\rm pg}(T_3)$  is the specific heat of gas at  $T_3$  which can be calculated by Eq. (5) [42].

$$C_{pg(T)} = 0.991615 + \left(\frac{6.99703T}{10^5}\right) + \left(\frac{2.7129T^2}{10^7}\right) - \left(\frac{1.22442T^3}{10^{10}}\right)$$
 (5)

where  $C_{pg(T)}$  is the specific heat of gas at temperature of T. The mass balance equation of the CC is presented as Eq. (6) [8].

$$\dot{m}_{g} = \dot{m}_{a} + \dot{m}_{\text{fuel}} \tag{6}$$

As shown in Fig. 4, since, there is a pressure drop in the CC  $(\Delta P_{CC})$ , the inlet pressure of the GT  $(P_3)$  is given by Eq. (7) [8].

$$\frac{P_3}{P_2} = (1 - \Delta P_{\rm cc}) \tag{7}$$

2.2.1.3. GT. As shown in Fig. 4, the actual outlet temperature of the GT  $(T_4)$  is more than the ideal outlet temperature  $(T_{4i})$  due to irreversibility during the expansion process. The outlet temperature of the GT is calculated by Eq. (8) [12].

$$T_4 = T_3 \left( 1 - \eta_{\rm GT} \left( 1 - r_{\rm GT}^{\frac{1 - \gamma_g}{\gamma_g}} \right) \right) \tag{8}$$

where  $T_3$ ,  $T_4$ ,  $\eta_{\rm GT}$ , and  $r_{\rm GT}$  are the inlet temperature, outlet temperature, isentropic efficiency, and the pressure ratio of the GT, respectively, and  $\gamma_g$  is the heat capacity ratio of gas. The power generation of the GT is given by Eq. (9) [8].

$$\dot{W}_{GT} = \dot{m}_g \Big( C_{pg(T_3)} T_3 - C_{pg(T_4)} T_4 \Big)$$
 (9)

where  $\dot{W}_{\rm GT}$  is the GT power generation,  $C_{{\rm pg}(T_3)}$  and  $C_{{\rm pg}(T_4)}$  are the specific heat of gas at  $T_3$  and  $T_4$  which are calculated by Eq. (5).

2.2.1.4. HRSG. The energy balance equation of the HRSG is presented as Eq. (10) [8].

$$\dot{m}_{17} \cdot (h_{19} - h_{17}) = \dot{m}_g \left( C_{pg(T_4)} T_4 - C_{pg(T_{18})} T_{18} \right)$$
 (10)

where  $C_{pg(T_4)}$  and  $C_{pg(T_{18})}$  are the specific heat of gas at  $T_4$  and  $T_{18}$  which are calculated by Eq. (5).

### 2.2.2. SWRO desalination subsystem

The SWRO subsystem is modeled by Eqs. (11)—(27), presented in Table 1. The water flux through the membrane is given by Eq. (11), where  $J_w$  is the water flux trough the membrane, A is the pure water permeability constant,  $P_b$  is brine stream pressure,  $P_p$  is permeate stream pressure, R is the ideal gas constant,  $T_{\rm sw}$  is seawater temperature,  $C_m$  is the wall mass salt concentration,  $C_p$  is permeate concentration, and  $M_s$  is the molecular weight of the solute. The salt flux through the membrane is given by Eq. (12), where  $J_s$  is the salt

**Table 1**Governing equations in the RO (reverse osmosis) system.

Equation		
		[43]
$J_{w} = 3600A \left( P_{b} - P_{p} - \frac{RT_{sw}\rho_{b}(C_{m} - C_{p})}{10^{6}M_{s}101325} \right)$	(11)	

$$J_{s} = \frac{3600B(C_{m} - C_{f})\rho_{b}}{10^{6}}$$
 (12)

$$C_p = \frac{J_s 10^6}{V_w \rho_p} \tag{13}$$

$$V_w = \frac{(J_w + J_s)}{\rho_p} \tag{14}$$

$$Q_p = V_w A_m \tag{15}$$

$$Q_f = Q_b + Q_D \tag{16}$$

$$Q_f C_f = Q_b C_b + Q_D C_D \tag{17}$$

$$\frac{C_m - C_p}{C_b - C_p} = \exp\left(\frac{V_w}{3600K_s}\right) \tag{18}$$

$$Sh = 0.664k_{dc}Re^{0.5}Sc^{0.33}\left(\frac{2d_h}{l}\right)^{0.5}$$
 (19)

$$Re = \frac{\rho d_h u}{u} \tag{20}$$

$$Sc = \frac{K_s d_h}{2}$$
 (21)

$$u = \frac{Q_b}{w h_{\rm sp} \varepsilon} \tag{22}$$

$$\Delta p = \frac{\rho u^2 L C_{\rm td}}{2 d_h} \tag{23}$$

$$C_{\rm td} = \frac{A'}{P e^{\pi}} \tag{24}$$

$$A = A_{\text{ref}}(\Delta \pi) \cdot \text{FF-TCF}$$
 (25)

TCF = 
$$\exp\left[2640\frac{1}{298} - \frac{1}{273 + T_f}\right]$$
  $T_f \ge 25 \,^{\circ}\text{C}$  (26)

TCF = 
$$\exp\left[3020\frac{1}{298} - \frac{1}{273 + T_f}\right]$$
  $T_f \le 25 \,^{\circ}\text{C}$  (27)

flux through the membrane,  $C_m$  is the wall mass salt concentration,  $C_f$  is feed water concentration, and  $\rho_b$  is density of the brine stream. The permeate concentration used in Eq. (11) is calculated by Eq. (13), where  $V_w$  is the permeate velocity that is given by Eq. (14). The permeate flow rate is given by Eq. (15), where  $Q_p$  is the permeate flow rate, and  $A_m$  is the membrane area. The mass and salt balance equations are Eqs. (16) and (17), respectively. The concentration polarization is an important phenomenon that reduces the fresh water flow rate and must be considered in the model. The film theory is used in this study to describe the concentration polarization [21]. According to the film theory, the concentration polarization can be modeled by Eq. (18).  $K_s$  is the mass transfer coefficient, which is calculated using the relationship between the Sherwood, Reynolds, and Schmidt numbers given by Eqs. (19)-(21). The Sherwood number is given by Eq. (19), and the Reynolds number is given by Eq. (20), where  $\rho$  is density,  $d_h$  is the hydraulic diameter of the feed spacer channel,  $\mu$  is the water viscosity, and *u* is the average velocity in the feed channel containing the baffle, which is calculated by Eq. (22). Pressure gradient across the membrane is given by Eq. (23), where  $\Delta p$  is the pressure gradient across the membrane, u is the average velocity in the feed channel containing the baffle, L is the length of the fiber bundle,  $d_h$ is the hydraulic diameter of the feed spacer channel, and  $C_{td}$  is the total drag force, which is calculated by Eq. (24). The membrane pure water permeability A (in Eq. (1)) is approximated as a function of feed water temperature, trans-membrane osmotic pressure, and FF (fouling factor) by Eq. (25), where A is the membrane pure water permeability,  $A_{\text{ref}}(\Delta \pi)$  is the reference permeability at  $T_0 = 298$  K, FF is the fouling factor, and TCF is the temperature correction factor at feed water temperature which is given by Eqs. (26) and (27). The influence of membrane fouling on the membrane permeability is expressed by the FF. Since, the membranes are assumed as new membranes, the FF is considered to equal 1. The membrane module constructed by Filmtech with trade name SW30HR-380 is used in the current study. The characteristics of the membrane module are presented in Table 2.

### 2.2.3. Refrigeration subsystems

2.2.3.1. Single-effect  $H_2O/LiBr$  absorption chiller subsystem. Fig. 5 shows T—s diagram of the single-effect water/LiBr absorption cycle [44] in the  $GT - AC_{H_2O-LiBr} - RO$  system. As shown in Figs. 3 and 5, the vapor refrigerant (stream 33) coming from the evaporator is absorbed by the strong solution (stream 29) and then leaves the absorber with a week LiBr concentration (stream 24). The released heat of the solution in the absorber is recovered to preheat the RO feed water (stream 16). The week solution is pumped to the desorber at a higher pressure through the SHX (solution heat

**Table 2** Characterization of the membrane element.

Membrane specific parameter	Unit	Value
Active area, $A_m$	m <sup>2</sup>	35
Length of the element, L	m	1.016
Diffusion coefficient, D	m <sup>2</sup> /s	$1 \times 10^{-9}$
Maximum operation pressure	bar	69
Pure water permeability constant, $A_{ref}$	kg/m² s Pa	$2.7 \times 10^{-9}$
Salt permeability constant, B	kg/m <sup>2</sup> s	$2.3 \times 10^{-5}$
Hydraulic diameter of the feed spacer channel, $d_h$	m	$8.126 \times 10^{-4}$
Length of the filament in the space mesh, <i>l</i>	m	$2.77 \times 10^{-3}$
Height of the feed spacer channel, $h_{sp}$	m	$5.93 \times 10^{-4}$
Void fraction of the spacer, $\varepsilon$	_	0.9
Baffle parameter, A'	_	7.38
Baffle parameter, n	_	0.34
Baffle parameter, $k_{\rm dc}$	_	1.05

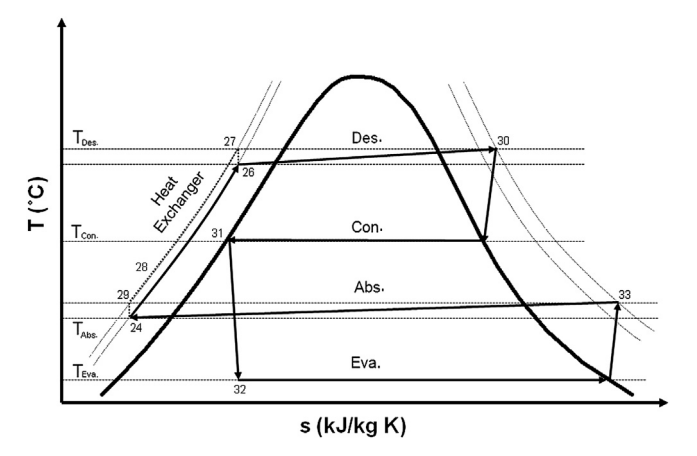


**Fig. 5.** Temperature–entropy (T-s) diagram of the  $AC_{H_2O-LiBr}$  cycle [44].

exchanger). The week solution (stream 25) is preheated by heat recovery from the strong solution (stream 27) coming from the desorber. In the desorber, the refrigerant is boiled off by adding heat provided by HRSG. The vapor (stream 30) is condensed through the condenser using cooling water and then flows to the evaporator through the refrigerant expansion valve to cool the compressor inlet air (stream 1). The strong liquid solution (stream 27) returns to the absorber through the SHX and expansion valve. The model equations for components of the AC<sub>H2O-LiBr</sub> subsystem, including desorber, condenser, absorber, evaporator, expansion valves, pump, and SHX, are Eqs. (28)–(43) [45,46]. Enthalpy and entropy for water/LiBr have been calculated by the correlations from Ref. [47].

Des. (desorber)

Mass, concentration, and energy balance equations are presented in Eqs. (28)–(30) [46].

$$\dot{m}_{26} = \dot{m}_{30} + \dot{m}_{27} \tag{28}$$

$$\dot{m}_{26}x_{26} = \dot{m}_{30}x_{30} + \dot{m}_{27}x_{27} \tag{29}$$

$$\dot{Q}_{\text{des.}} = \dot{m}_{30}h_{30} + \dot{m}_{27}h_{27} - \dot{m}_{26}h_{26} \tag{30}$$

where  $\dot{m}$  is the mass flow rate, x is the solution concentration, and  $\dot{Q}_{des.}$  is the heat requirement of the desorber.

Eva.<sub>AC</sub> (evaporator)

Mass, and energy balance equations are shown in Eqs. (31) and (32), respectively [48].

$$\dot{m}_{32} = \dot{m}_{31} \tag{31}$$

$$\dot{Q}_{\text{eva.ac}} = \dot{m}_{32} h_{32} - \dot{m}_{31} h_{31} \tag{32}$$

where  $\dot{Q}_{\text{eva.}_{AC}}$  is the cooling load of the evaporator, and h is the enthalpy.

Cond.<sub>AC</sub> (condenser)

Mass, and energy balance equations are presented in Eqs. (33) and (34), respectively [48].

$$\dot{m}_{30} = \dot{m}_{31} \tag{33}$$

$$\dot{Q}_{\text{con,ac}} = \dot{m}_{30} h_{30} - \dot{m}_{31} h_{31} \tag{34}$$

where  $\dot{Q}_{con._{AC}}$  is the waste heat of the condenser.

Abs. (absorber)

Mass, concentration, and energy balance equations are presented in Eqs. (35)–(37), respectively [46].

$$\dot{m}_{24} = \dot{m}_{32} + \dot{m}_{29} \tag{35}$$

$$\dot{m}_{24}x_{24} = \dot{m}_{32}x_{32} + \dot{m}_{29}x_{29} \tag{36}$$

$$\dot{Q}_{abs,ac} = \dot{m}_{32}h_{32} + \dot{m}_{29}h_{29} - \dot{m}_{24}h_{24} \tag{37}$$

where  $\dot{Q}_{abs,ac}$  is the released heat in the evaporator.

SHX

The energy balance equation is shown in Eq. (38) [48].

$$\dot{m}_{25}(h_{25} - h_{26}) = \dot{m}_{27}(h_{28} - h_{27}) \tag{38}$$

Exp. (expansion valves)

Mass, and energy balance equations for refrigerant expansion valve are given by Eqs. (39) and (40), respectively [46].

$$\dot{m}_{31} = \dot{m}_{32} \tag{39}$$

$$\dot{m}_{31}h_{31} = \dot{m}_{32}h_{32} \tag{40}$$

Mass, and energy balance equations for solution expansion valve are given by Eqs. (41) and (42), respectively [46].

$$\dot{m}_{28} = \dot{m}_{29} \tag{41}$$

$$\dot{m}_{28}h_{28} = \dot{m}_{29}h_{29} \tag{42}$$

Solution pump

The power consumption of the solution pump is given by Eq. (43) [48].

$$\dot{W}_{\text{pump}} = \dot{m}_{24}(h_{25} - h_{24}) \tag{43}$$

2.2.3.2. VCR subsystem. The T—s diagram of the VCR cycle in the GT—VCR—RO system is presented in Fig. 6. As shown in Fig. 6, the saturated vapor refrigerant is compressed by an irreversible compression process (line 13—14). The compressed vapor is condensed through the condenser (line 14—15) and the released heat is recovered to preheat the RO feed water. The refrigerant leaves condenser as the saturated liquid vapor at lower pressure than that of the compressor outlet due to unavoidable pressure drop in the condenser. The saturated liquid refrigerant enters the evaporator through the expansion valve to cool the inlet air of the GT compressor. The cycle is completed as the refrigerant exits from

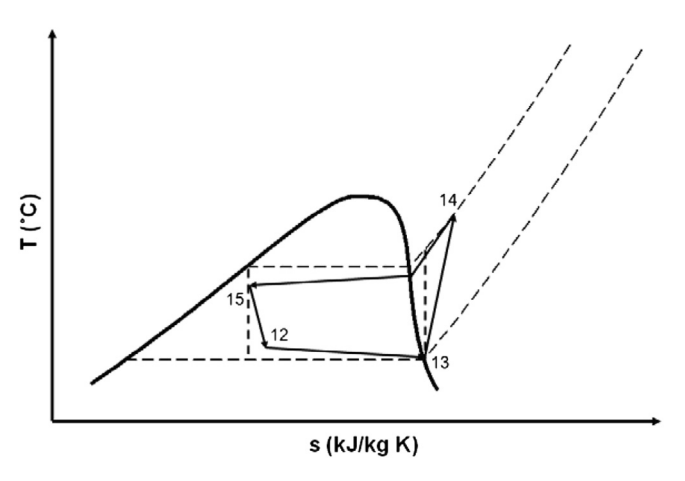


**Fig. 6.** Temperature—entropy (*T*–*s*) diagram of the VCR cycle.

the evaporator as saturated vapor at lower pressure than that of the expansion valve outlet due to the pressure drop in the evaporator [49]. The mathematical equations for components of the VCR subsystem, including compressor, evaporator, condenser, and expansion valve are Eqs. (44)–(47).

Eva.<sub>VCR</sub> (evaporator)

The energy balance equation is presented in Eq. (44) [8].

$$\dot{Q}_{\text{eva.}_{\text{VCR}}} = \dot{m}_{\text{ref.}}(h_{13} - h_{12}) \tag{44}$$

where  $\dot{Q}_{\rm eva._{VCR}}$  is the cooling load of the evaporator,  $\dot{m}_{\rm ref.}$  is the refrigerant mass flow rate, and h is the enthalpy.

Com.<sub>VCR</sub> (compressor)

The power consumption of the compressor is given by Eq. (45) [5].

$$\dot{W}_{\text{com,vcr}} = \dot{m}_{\text{ref}} \left( h_{14} - h_{13} \right) \tag{45}$$

where  $\dot{W}_{com._{VCR}}$  is power consumption of the compressor.

Expansion valve

Energy balance equation for the expansion valve is given by Eq. (46) [8].

$$\dot{m}_{\rm ref} \, h_{15} = \dot{m}_{\rm ref} \, h_{12} \tag{46}$$

Con.<sub>VCR</sub> (condenser)

The energy balance equation for the VCR condenser is given by Eq. (47) [5].

$$\dot{Q}_{\text{con,vcp}} = \dot{m}_{\text{ref.}} (h_{14} - h_{15}) \tag{47}$$

where  $\dot{Q}_{con._{VCR}}$  is the waste heat from the condenser.

The initial circumstances for the operating and thermodynamic parameters for the GT power plant, VCR, and  $AC_{H_2O-LiBr}$  subsystems are presented in Table 3.

**Table 3** Operating parameters and thermodynamic parameters' initial circumstances for GT power plant, VCR, and  $AC_{H_2O-LiBr}$  subsystems.

Parameter	Value	Unit
GT subsystem		
$T_{air}$	35	°C
RH	30	%
$m_{ m air}$	0.3	kg/s
$m_{ m fuel}$	0.007	kg/s
$r_{\rm ac}$	6	_
$\eta_{ m com}$	91	%
$\eta_{ ext{GT}}$	91	%
$\eta_{ m cc}$	90	%
LHV	51,400	kJ/kg
VCR subsystem		
$\Delta T_{\min, \text{Eva}}$	10	°C
Refrigerant	R-134a	_
$r_{\rm com}$	3.5	_
$\eta_{ m com}$	91	%
X <sub>13</sub>	1	_
X <sub>15</sub>	0	_
GT-AC <sub>H2O-LiBr</sub> -RO subs		
$\Delta T_{ m min,Eva}$	10	°C
$\Delta T_{ m min,con}$	10	°C
$\Delta T_{\rm min,abs}$	10	°C
$\Delta T_{ m min,des}$	10	°C
$\eta_{ m pump}$	91	%
X <sub>13</sub>	1	_
$X_{15}$	0	_
$P_{ m high}$	7.44	kPa
$P_{low}$	0.67	kPa

### 2.3. Exergy analysis of cogeneration systems

Exergy is a measure of the maximum capacity of a system to perform useful work as it proceeds to a specified final state in equilibrium with its surrounding. Exergy can be divided into four distinct components. The two important ones are the physical exergy and chemical exergy; the two other components of kinetic exergy and potential exergy are assumed to be negligible in this study [20,50]. The physical exergy is defined as the theoretical maximum of useful work obtained as a system interacts in an equilibrium state. The chemical exergy is associated with the departure of the chemical composition of a system from its chemical equilibrium. The chemical exergy is an important part of exergy in combustion processes [41].

## 2.3.1. Exergy balance equations in the GT power plant and refrigeration chillers

Based on the first and second laws of thermodynamics, the following exergy balance equation is obtained [20]:

$$\dot{E}x_{Q} + \sum_{i} \dot{E}x_{i} = \sum_{e} \dot{E}x_{e} + \dot{E}x_{w} + \dot{E}x_{D}$$
(48)

where subscripts e and i represent inlet and outlet specific exergy of the control volume, respectively, and  $\dot{E}x_D$  is the exergy destruction. Other terms in this equation are as follows [23,24]:

$$\dot{E}x_{Q} = \left(1 - \frac{T_{0}}{T_{i}}\right)\dot{Q}_{i} \tag{49}$$

$$\dot{E}x_{W} = \dot{W} \tag{50}$$

$$\dot{E}x = \dot{m}ex$$
 (51)

$$\dot{E}x = \dot{E}x_{\rm ph} + \dot{E}x_{\rm ch} \tag{52}$$

$$\dot{E}x_{\rm ph} = (h - h_0) - T_0(s - s_0) \tag{53}$$

where  $\dot{E}x_Q$  and  $\dot{E}x_W$  are the corresponding exergies of the heat transfer and work that cross the boundaries of the control volume, T is temperature (K), and (0) refers to the ambient conditions. The mixture's chemical exergy is defined as follows [40]:

$$ex_{mix}^{ch} = \left[ \sum_{i=1}^{n} X_i ex^{ch_i} + RT_0 \sum_{i=1}^{n} X_i LnX_i \right]$$
 (54)

For the evaluation of the fuel exergy, the following exergy ratio is used [20]:

$$\xi = \frac{ex_{\text{fuel}}}{LHV_{\text{fuel}}} \tag{55}$$

For most of the commonly used gaseous fuels, the ratio of chemical exergy to lower heating value is usually close to 1. Since in this study the fuel used in the GT power plant is methane, therefore  $\xi$  is calculated as 1.06 [20,40].

### 2.3.2. Exergy balance equation of the SWRO desalination system

The specific entropy and enthalpy of a component per unit mole in an ideal solution at a specified temperature *T* and pressure *P* are as follows [40]:

$$h = mf_s h_s + mf_w h_w (56)$$

$$s = mf_s + mf_w s_w (57)$$

where subscripts s and w represent salt and water, and  $m_f$  is mass fraction. The assumed conditions of the environment are as follows. The seawater inlet for desalination is at temperature of 298 K, air pressure of 1 atm, and salinity of 0.042%. The specific heat, the enthalpy, and the entropy of the salt at  $T_0 = 298$  K are  $cp_s = 0.8368$  kJ/kg K,  $h_{s_0} = 20.92$  kJ/kg, and  $S_{s_0} = 0.0732978$ , respectively. Therefore, the enthalpy and entropy of the salt at temperature T can be determined by Eqs. (58) and (59) [40]

$$h_s = h_{s_0} + cp_s(T - T_0) = 20.92 + 0.8368(T - 298)$$
 (58)

$$S_s = S_{s_0} + cp_s ln(T/T_0) = 0.0732978 + 0.8368ln(T/298)$$
 (59)

Mixing is an irreversible process, and thus the entropy of a mixture at a specified temperature and pressure must be greater than the sum of the entropies of the individual components (before mixing) at the same temperature and pressure. The entropy of the component per unit mole in an ideal solution at a specified temperature *T* and pressure *P* is given by Eq. (60) [21].

$$\bar{s}_i = \bar{s}_{i,\text{pure}}(T, P) - R_u \ln x_i \tag{60}$$

The entropy of a saline solution, which is the sum of the entropies of the salt and water in the saline solution, is given by Eq. (61) [26].

$$\overline{s} = x_s \overline{s}_s + x_w \overline{s}_w 
= x_s [s_{s,pure}(T, P) - R_u ln x_s] + x_s [s_{w,pure}(T, P) - R_u ln x_w] 
= x_s s_{s,pure}(T, P) + x_w s_{w,pure}(T, P) - R_u (x_s ln x_s + x_w ln x_s)$$
(61)

The entropy of saline water per unit mass is determined by Eq. (62) [21].

$$s_{sw} = mf_s s_{s,pure}(T, P) + mf_w s_{w,pure}(T, P) - R_u(x_s \ln x_s + x_w \ln x_w)$$
(62)

The exergy of a flow stream is given by Eq. (63) [23].

$$ex = h - h_0 - T_0(s - s_0) (63)$$

Then, the rate of exergy flow associated with a flow stream is determined by Eq. (64) [23].

$$\dot{E}x = \dot{m}[h - h_0 - T_0(s - s_0)] \tag{64}$$

# 2.3.3. Definition of exergy and energy efficiencies and net power generation of cogeneration systems

The first-law efficiency of each system is expressed in Eq. (65) as the work or energy delivered, divided by the work or energy input [8].

$$\eta_{\text{energetic}} = \frac{\dot{E}_{\text{delivered}}}{\dot{E}_{\text{input}}} \tag{65}$$

The net power generation of each system is calculated as the GT power generation minus power consumption of the total system in Eq. (66) [5].

$$\dot{W}_{\text{net}} = \dot{W}_{\text{GT}} - \dot{W}_{\text{consumption}}$$
 (66)

The second-law efficiency of each component is the ratio of the minimum exergy input required (which is equivalent to the minimum work) to the total actual exergy input in Eq. (67) [8].

$$\eta_{\text{exergetic}} = \frac{\dot{W}_{\text{min}}}{\dot{E}x_{\text{in,total}}} = \frac{\dot{E}x_{\text{out}} - \dot{E}x_{\text{in}}}{\dot{E}x_{\text{in,total}}}$$
(67)

Therefore, the overall exergy efficiencies of the three considered systems are determined by Eqs. (68)–(70).

$$\eta_{\text{exergetic}_{\text{first,system}}} = \frac{\dot{W}_{\text{net}_{\text{first,system}}} - \dot{E}x_8 + \dot{E}x_9 - \dot{E}x_6}{\dot{E}x_f + \dot{E}x_1}$$
(68)

$$\eta_{\text{exergetic}_{\text{second,system}}} = \frac{\dot{W}_{\text{net}_{\text{second,system}}} + \dot{E}x_8 + \dot{E}x_9 - \dot{E}x_6}{\dot{E}x_f + \dot{E}x_{11}}$$
(69)

$$\eta_{\text{exergetic}_{\text{third,system}}} = \frac{\dot{W}_{\text{net}_{\text{third,system}}} + \dot{E}x_8 + \dot{E}x_9 - \dot{E}x_6}{\dot{E}x_f + \dot{E}x_{11}}$$
(70)

### 2.4. Parametric analysis and optimization of cogeneration systems

To evaluate the effect of each major parameter on the cogeneration system performance, parametric analysis is conducted. Parametric analysis of a cogeneration system shows its potential to be optimized. For practical operation, the cogeneration systems have many parameters that vary together, presenting a multi-dimensional surface on which an optimal set of values can be found [19,22]. In the present study, the overall exergy efficiency, was selected as an objective function of the parameter optimization in each cogeneration system (Eqs. (68)—(70)), because it can evaluate the performance of the cogeneration systems. Parameter

optimization was achieved using a GA of MATLAB 7.11 to reach the maximum exergy efficiency.

In thermal system optimization, it is useful to identify two types of independent variables which are decision variables and parameters. The decision variables are those that must be decided in the optimization process. The parameters are the variables that remain fixed in a given system. All other variables are dependent variables which are calculated from independent variables with thermodynamic relationships [51]. In this study, the decision variables for the three systems are the compressor inlet air temperature  $(T_1)$  and the fuel-mass flow rate  $(m_{\text{fuel}})$ . The operation ranges of each variable are selected based on the working ranges of the various parameters in the cogeneration systems. The constraints of the parameters are summarized in Table 4. Since the systems are optimized under the same constraints for variables, the theoretical conditions are just considered for rages of the constraints but not the practical conditions. To satisfy the economic aspect of the heat exchangers, the heat transfer temperature difference between the cold and hot streams was chosen to be equal or greater than 10 °C.

### 2.4.1. GA

A GA is a parallel, iterative, and population-based search used to find the optimal solution in a large solution domain by carrying out stochastic transformations inspired by natural evolution [52-54]. The GA considers parameters as genes that form chromosomes which represent solutions. Each gene controls one or more features of its chromosome. A collection of chromosomes creates a population. With a randomly generated population, the algorithm begins using three genetic operators: selection, crossover, and mutation. Based on values of the individuals, the chromosomes are selected for transition from the current population by a selection process that is called the selection operator. The crossover operator combines two chromosomes, called parents, to generate two similar children. The crossover operator continues this process until it completes the generation [55–58]. Because the selection and crossover may become overzealous, the mutation operator performs random changes in the genes of existing chromosomes [59]. Together, these processes (selection, crossover, and mutation) are referred to as one generation. The generational cycle stops when a desired termination criterion is achieved [4].

**Table 4**Optimization constraints of cogeneration systems.

$ \begin{array}{c ccccccccccccccccccccccccccccccccccc$	Parameter	Constraints	Reason							
$\begin{array}{c ccccccccccccccccccccccccccccccccccc$	GT-VCR-RO system									
$\begin{array}{c ccccccccccccccccccccccccccccccccccc$	$T_1$	$14.84 \le m_{\text{fuel}} \le 35$ °C	Dew point							
$T_{2} = 1000000000000000000000000000000000000$	$m_{\mathrm{fuel}}$	$0.007 \le m_{\text{fuel}} \le 0.02 \text{ kg/s}$	Availability							
$\begin{array}{cccccccccccccccccccccccccccccccccccc$	$T_4$	≥140 °C	To avoid formation of sulfuric							
$\begin{array}{c ccccc} \Delta T_{\rm Eva} & = 10~^{\circ}{\rm C} & {\rm Commercial~justification} \\ \Delta T_{\rm con} & \geq 10~^{\circ}{\rm C} & {\rm Commercial~justification} \\ GT-{\rm AB-RO~system} & & & & & \\ T_1 & 14.84 \leq m_{\rm fuel} \leq 35~^{\circ}{\rm C} & {\rm Dew~point} \\ m_{\rm fuel} & 0.007 \leq m_{\rm fuel} \leq 0.02~{\rm kg/s} & {\rm Availability} \\ T_{18} & \geq 140~^{\circ}{\rm C} & {\rm To~avoid~formation~of~sulfuric~acid~in~exhaust~gases} \\ T_3 & \leq 1280~^{\circ}{\rm C} & {\rm Material~temperature~limit} \\ \Delta T_{\rm Des.} & = 10~^{\circ}{\rm C} & {\rm Commercial~justification} \\ \Delta T_{\rm Eva.} & = 10~^{\circ}{\rm C} & {\rm Commercial~justification} \\ \Delta T_{\rm Con} & = 10~^{\circ}{\rm C} & {\rm Commercial~justification} \\ \Delta T_{\rm Abs.} & = 10~^{\circ}{\rm C} & {\rm Commercial~justification} \\ \end{array}$			acid in exhaust gases							
$\begin{array}{lllll} \Delta T_{\text{con}} & \geq 10  ^{\circ}\text{C} & \text{Commercial justification} \\ GT-AB-RO  \text{system} & & & & \\ T_1 & 14.84 \leq m_{\text{fuel}} \leq 35  ^{\circ}\text{C} & \text{Dew point} \\ m_{\text{fuel}} & 0.007 \leq m_{\text{fuel}} \leq 0.02   \text{kg/s} & \text{Availability} \\ T_{18} & \geq 140  ^{\circ}\text{C} & \text{To avoid formation of sulfuric acid in exhaust gases} \\ T_3 & \leq 1280  ^{\circ}\text{C} & \text{Material temperature limit} \\ \Delta T_{\text{Des.}} & = 10  ^{\circ}\text{C} & \text{Commercial justification} \\ \Delta T_{\text{Eva.}} & = 10  ^{\circ}\text{C} & \text{Commercial justification} \\ \Delta T_{\text{con}} & = 10  ^{\circ}\text{C} & \text{Commercial justification} \\ \Delta T_{\text{Abs.}} & = 10  ^{\circ}\text{C} & \text{Commercial justification} \\ \end{array}$	T <sub>3</sub>	≤1280 °C	Material temperature limit							
$\begin{array}{cccccccccccccccccccccccccccccccccccc$	$\Delta T_{\text{Eva}}$	=10 °C	Commercial justification							
$\begin{array}{cccccccccccccccccccccccccccccccccccc$	$\Delta T_{ m con}$	≥10 °C	Commercial justification							
$\begin{array}{cccccccccccccccccccccccccccccccccccc$	GT-AB-RO sy	ystem								
$\begin{array}{c ccccccccccccccccccccccccccccccccccc$	$T_1$	$14.84 \le m_{\mathrm{fuel}} \le 35  ^{\circ}\mathrm{C}$	Dew point							
$\begin{array}{cccccccccccccccccccccccccccccccccccc$	$m_{\mathrm{fuel}}$	$0.007 \le m_{\text{fuel}} \le 0.02 \text{ kg/s}$	Availability							
$\begin{array}{lll} T_3 & \leq 1280 \ ^{\circ}\text{C} & \text{Material temperature limit} \\ \Delta T_{\text{Des.}} & = 10 \ ^{\circ}\text{C} & \text{Commercial justification} \\ \Delta T_{\text{Eva.}} & = 10 \ ^{\circ}\text{C} & \text{Commercial justification} \\ \Delta T_{\text{con}} & = 10 \ ^{\circ}\text{C} & \text{Commercial justification} \\ \Delta T_{\text{Abs.}} & = 10 \ ^{\circ}\text{C} & \text{Commercial justification} \end{array}$	$T_{18}$	≥140 °C	To avoid formation of sulfuric							
$\begin{array}{lll} \Delta T_{Des.} & = 10  ^{\circ} \text{C} & \text{Commercial justification} \\ \Delta T_{Eva.} & = 10  ^{\circ} \text{C} & \text{Commercial justification} \\ \Delta T_{con} & = 10  ^{\circ} \text{C} & \text{Commercial justification} \\ \Delta T_{Abs.} & = 10  ^{\circ} \text{C} & \text{Commercial justification} \end{array}$			acid in exhaust gases							
$\begin{array}{lll} \Delta T_{Eva.} & = 10 \ ^{\circ} C & Commercial justification \\ \Delta T_{con} & = 10 \ ^{\circ} C & Commercial justification \\ \Delta T_{Abs.} & = 10 \ ^{\circ} C & Commercial justification \\ \end{array}$	$T_3$	≤1280 °C	Material temperature limit							
$\Delta T_{\text{con}}$ = 10 °C Commercial justification $\Delta T_{\text{Abs.}}$ = 10 °C Commercial justification	$\Delta T_{\mathrm{Des.}}$	=10 °C	Commercial justification							
$\Delta T_{\text{Abs.}}$ =10 °C Commercial justification	$\Delta T_{\mathrm{Eva.}}$	=10 °C	Commercial justification							
	$\Delta T_{\rm con}$	=10 °C	Commercial justification							
	$\Delta T_{\mathrm{Abs.}}$	=10 °C	Commercial justification							
$\Delta T_{\text{HRSG}}$ $\geq 10 ^{\circ}\text{C}$ Commercial justification	$\Delta T_{ m HRSG}$	≥10 °C	Commercial justification							

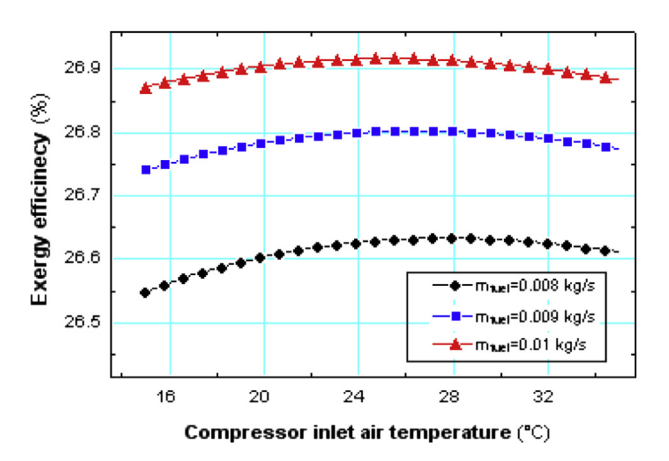
### 3. Results and discussion

### 3.1. Parametric analysis and optimization results

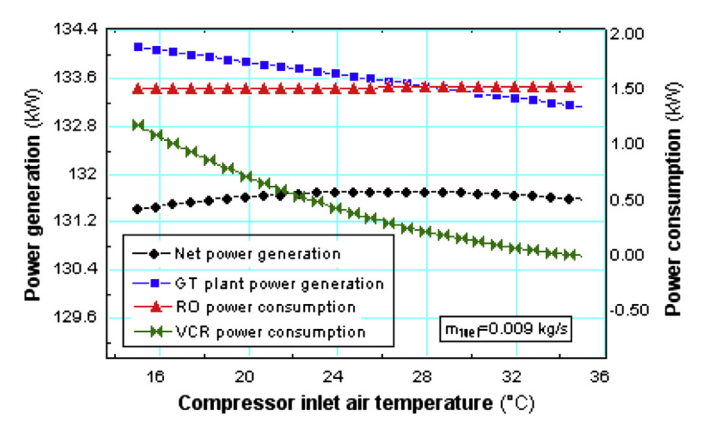
Parametric analysis was performed to evaluate the effects of two key parameters—the compressor inlet air temperature  $(T_1)$  and the mass flow rate of fuel  $(m_{\rm fuel})$ —on the exergy efficiency of cogeneration systems. In the parametric analysis, one parameter was varied, while the other was kept constant.

Fig. 7 shows the effect of the compressor inlet air temperature on the exergy efficiency of the GT-VCR-RO system (the second system). At a fixed fuel-mass flow rate, the system exergy efficiency increases with the decrease of compressor inlet air temperature to around 26 °C and then decreases with the decrease of compressor inlet air temperature. Because, based on the exergy efficiency equation of the second system presented in Eq. (69), the exergy efficiency of the system has a direct relationship with the net power generation of the system. Since the net power generation of the system increases and decreases with the decrease of compressor inlet air temperature, therefore the system exergy efficiency increases and decreases with the decrease of compressor inlet air temperature. Fig. 8 shows the effect of compressor inlet air temperature on the net power generation of the GT-VCR-RO system. As shown in Fig. 8, at a fixed value of fuel-mass flow rate, the system net power generation increases with the increase of compressor inlet air temperature until the exergy efficiency of the system reaches its maximum value and then it decreases. Increase and decrease in system net power generation lead to increase and decrease in system exergy efficiency, as shown in Fig. 7. Because the net power generation is depended on the GT net power generation, the RO power consumption, and the VCR power consumption, the net power generation is estimated by investigating these three power variations with respect to the compressor inlet air temperature. As shown in Fig. 8, the power consumption of the RO is linearly decreased with the decrease of compressor inlet air temperature and the power consumption of the refrigeration compressor is nonlinearly increased, while the net power generation of the GT increases. It represents that the system net power generation has a nonlinear (increase-then-decrease) relationship with the compressor inlet air temperature.

Increase of the VCR's compressor power consumption with the decrease of compressor inlet air temperature is due to the increase of the cooling load of the evaporator. Decrease of the power consumption in the RO system is due to increase in feed water temperature. This is because a decrease of compressor inlet air



**Fig. 7.** Effect of compressor inlet air temperature on system exergy efficiency at fixed fuel-mass flow rates for GT-VCR-RO system (second system).

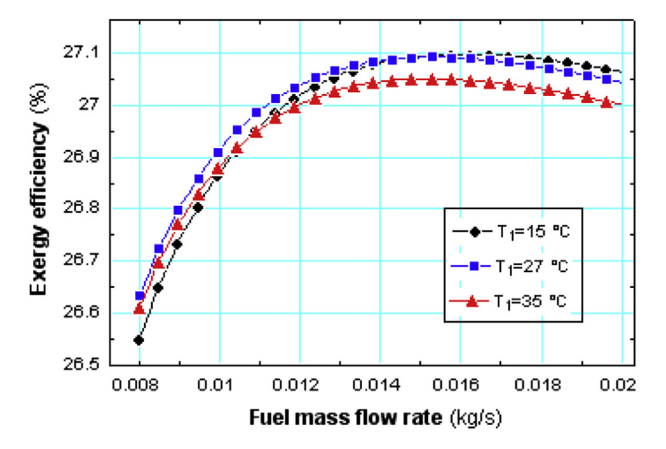


**Fig. 8.** Effect of compressor inlet temperature on system net power generation, RO power consumption, VCR power consumption, and GT net power generation at fixed fuel-mass flow rate for GT–VCR–RO system (second system).

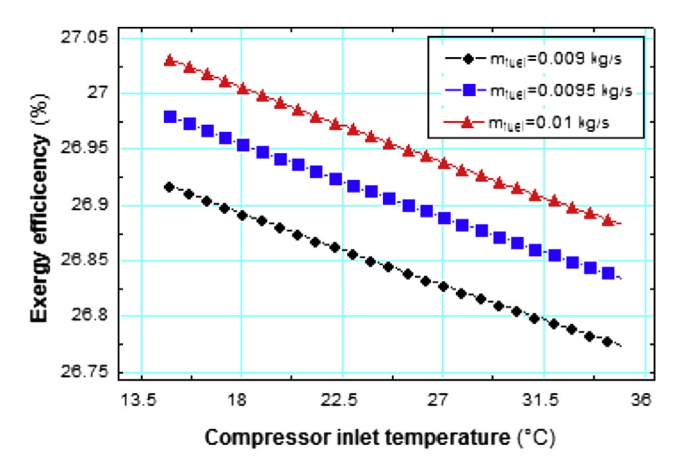
temperature results in an increase of the evaporator cooling load, which results in an increase of waste heat from the condenser. Since the waste heat from the condenser was recovered to preheat the feed water of the RO system, therefore decrease of compressor inlet air temperature results in decrease of RO power consumption, indirectly. Increase of GT net power generation with decrease of compressor inlet air temperature is due to increase of air density. Because the GT machines are constant-volume machines, increase of air density results in increases in air mass flow rate, thereby increasing GT power generation.

Fig. 9 shows the effect of the fuel-mass flow rate on the system exergy efficiency at the fixed compressor inlet air temperature. Increase of fuel-mass flow rate results in increase of exergy efficiency until a given fuel-mass flow rate is reached, and then further increase in fuel-mass flow rate results in decreasing exergy efficiency. On the other hand, at a fixed fuel-mass flow rate, exergy efficiency increases and decreases with increase in fuel-mass flow rate, as already discussed by Fig. 7.

Fig. 10 shows the effect of the compressor inlet air temperature on the system exergy efficiency for the GT - AC $_{\rm H_2O-LiBr}$  - RO system (third system). At a fixed fuel-mass flow rate, the system exergy efficiency increases with the decrease of compressor inlet air temperature. This can be explained through investigation of variations of the net power generation with respect to compressor inlet air temperature, as shown in Fig. 11: the net power generation of the GT subsystem increases with the decrease of



**Fig. 9.** Effect of fuel-mass flow rate on system exergy efficiency at fixed compressor inlet air temperatures for GT–VCR–RO system (second system).



**Fig. 10.** Effect of compressor inlet air temperature on the system exergy efficiency at fixed fuel-mass flow rate for  $GT-AC_{H_2O-LiBr}-RO$  system (third system).

compressor inlet air temperature. Also, the power consumption of the system, which is the sum of the RO pump and AC pump power consumptions, decreases with the decrease of the compressor inlet air temperature. The system power consumption decreases because when the compressor inlet air temperature decreases, the evaporator cooling load increases, and so the waste heat of the absorber increases. Since the absorber waste heat is recovered to preheat the RO feed water, the power consumption of the RO decreases. On the other hand, the power consumption of the AC pump increases with the increase of evaporator cooling load. Since the decrease in RO pump power consumption is greater than that of the AC pump, the net power consumption of the system decreases. The net power generation of the system increases, since the net power generation of the GT subsystem increases and the power consumption of the system decreases with decrease in the compressor inlet air temperature. As shown in Fig. 10, increase of the system net power generation leads to increase of the system exergy efficiency.

Fig. 12 shows the effect of the fuel-mass flow rate on the system exergy efficiency for the  $GT-AC_{H_2O-LiBr}-RO$  system. At a fixed compressor inlet air temperature, as the fuel-mass flow rate increases, the system exergy efficiency increases until maximum exergy efficiency is reached and then it decreases. It represents that the system exergy efficiency increases as the compressor inlet air temperature decreases, which was discussed by Fig. 10.

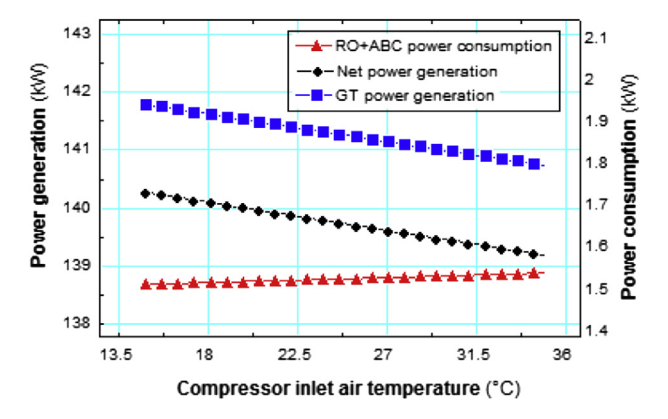


**Fig. 11.** Effect of compressor inlet air temperature on the net power generation of system, power consumption of RO, and net power generation of GT for  $GT-AC_{H_2,O-LiBr}-RO$  system at fixed fuel-mass flow rate of 0.0095 kg/s.

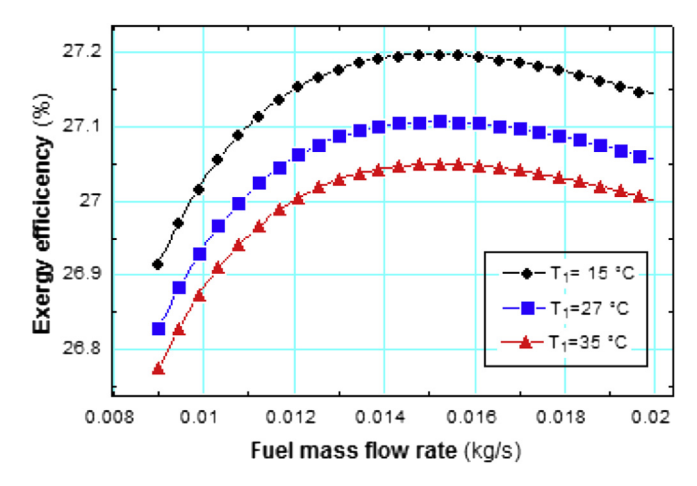


**Fig. 12.** Effect of fuel-mass flow rate on the system exergy efficiency at fixed compressor inlet air temperatures for  $GT-AC_{H_2O-LiBr}-RO$  system (third system).

Parametric analysis results of the systems indicate that, compressor inlet air temperature and fuel-mass flow rate have great influences on the system exergy efficiency. Therefore, parameter optimization using a GA was conducted to obtain the optimal operation conditions of the systems for maximum system exergy efficiency. Table 5 lists the optimization results of the decision variables of the compressor inlet air temperature  $(T_1)$  and the fuelmass flow rate ( $m_{\text{fuel}}$ ). As presented in Table 5, the compressor inlet air temperature of the GT-VCR-RO system (second system) and  $GT - AC_{H_2O-IiRr} - RO$  system (third system) is decreased until 26.43 °C and 14.84 °C and the fuel-mass flow rate is increased until 0.0093 and 0.0098 kg/s. Table 6 compares the exergy efficiency, energy efficiency, and net power generation of the optimized cogeneration systems. The results show that the GT-VCR-RO system (second system) and the GT – AC<sub>H2O-LiBr</sub> – RO (third system) are capable to increase the exergy efficiency by 2.89% and 3.79%, respectively, compared to the GT-RO system (first system). Also, the GT-VCR-RO and GT -  $AC_{H_2O-LiBr}$  - RO systems are able to increase the energy efficiency by 3.22% and 4.21% and net power generation by 32% and 38% respectively, compared to the GT-RO system. The increase of the net power generation of the second and third systems is not only due to the variations of the compressor inlet air temperature, but also due to the variations of the fuel-mass flow rate, because as presented in Table 5, the optimal values of the fuel consumption in the second and third systems were obtained 0.0093 and 0.0098 kg/s respectively which are more than that of the first system and the optimal values of the compressor inlet air

**Table 5**Optimal operation parameters values of cogeneration systems.

Parameter	Constraints
GT-VCR-RO system (second	system)
$T_1$	26.43 °C
$m_{ m fuel}$	0.0093 kg/s
$T_4$	785.7 °C
$T_3$	1279 °C
$\Delta T_{ m con}$	11.17 °C
ACH2O-LiBr system (third system	em)
$T_1$	14.84 °C
$m_{ m fuel}$	0.0098 kg/s
$T_{18}$	561 °C
$T_3$	1275 °C
$\Delta T_{ m HRSG}$	91 °C

**Table 6**Comparison of exergy, energy efficiencies and net power generation of cogeneration systems.

Cogeneration system	Exergy efficies	Exergy efficiency (%)		Energy efficiency (%)		Net power generation (kW)	
	Exergy efficiency	Compared to first system (capability) (%)	Energy efficiency	Compared to first system (%)	Net power generation	Compared to first system (%)	
GT-RO (first system)	26.31		27.69		99.7		
GT-VCR-RO (second system)	29.2	2.89	30.91	3.22	147.7	32	
$GT - AC_{H_2O-LiBr} - RO$ (third system)	30.1	3.79	31.9	4.21	161.6	38	

**Table 7**Results of thermodynamic simulation for GT—RO system (first system).

Sub system	Component	State point	Pressure (kPa)	Temperature (°C)	Mass flow rate (kg/s)	Specific enthalpy (kJ/kg)	Energy (kW)	Exergy (Kw)
GT	Com.	1	101	35	0.3426	308.52	105.7	0
		2	606	258.4	0.3426	553.61	183.5	82.09
	CC	2	606	258.4	0.3426	553.61	183.5	82.09
		5	700	35	0.007	51,428	360	381.6
		3	606	1100	0.3496	1482.55	518.3	358.7
	GT	3	606	1100	0.3496	1482.55	518.3	358.7
		4	103	657.2	0.3496	967.1	338.1	134.3
RO	Pump	6	101	25	0.3333	101.32	33.77	0
		7	5835	25.01	0.3333	106.39	35.46	1.844
	Mem.	7	5835	25.01	0.3333	106.39	35.46	1.844
		8	171	25.01	0.1	104.8	10.48	1.679
		9	4335	25.01	0.2333	103.514	24.15	-0.9724

temperature in the second and third systems were obtained 26.43 °C and 14.84 °C which are less than that of the first system. Since the GT –  $AC_{H_2O-LiBr}$  – RO system can increase exergy and energy efficiencies as well as net power generation more than those of the GT–VCR–RO and the GT–RO systems, the GT –  $AC_{H_2O-LiBr}$  – RO system is the best system among systems from the viewpoint of thermodynamics.

### 3.2. Exergy analysis of cogeneration systems

The thermodynamic model presented in Section 2.2 was used to calculate the thermodynamic properties of the three cogeneration systems, and exergy analysis was performed to evaluate their exergy destructions of the components.

Table 7 presents the simulation results of the GT–RO system (first system) and Table 8 lists the exergy inputs and outputs as well as exergy destructions. It was found that 73.69% of the total system input exergy was destructed: 73.16% in the GT power plant subsystem and 0.53% in the RO subsystem. In the GT power plant subsystem, 1.084%, 42.66%, and 1.586% of the total system exergy input were destructed in the air compressor, the CC, and the GT because of the irreversibility of the compression, combustion, and

**Table 8**Results of exergy analysis for GT—RO system (first system).

		Component	Amount (kW)		Percentage (%)	
Exergy input Exergy output			381.6 100.4		100 26.31	
Exergy destruction	GT	Air compressor Combustion	4.136 162.8	279.19	1.084 42.66	73.16
	RO	chamber Gas turbine Exhaust RO pump Membrane	6.054 106.2 0.2597 1.137	2.01	1.586 27.83 0.068 0.3	0.53
		Discharge	0.61		0.16	

expansion processes, where 27.83% of the input exergy was discharged to the environment through the exhaust. It was also found that, 0.068%, and 0.3% of the total system exergy input in the RO subsystem was destructed in the RO pump and the membrane due to the irreversibility of the pumping process and the pressure drop in the separation process. Note that 0.61% of the total exergy input was discharged to the environment, by discharging permeate and the high pressure brine streams.

For the GT-VCR-RO system (second system), Tables 9 and 10 list the simulation and exergy analysis results, respectively. It can be seen in Table 10 that 70.8% of the total input exergy is destructed: 70.48% in the GT power plant, 0.266% in the RO system and 0.059% in the VCR system. In the GT power plant, 39.52%, 1.23%, and 0.84% of the total system exergy input were destructed in the CC, the GT, and the air compressor, respectively, due to irreversibility of the processes, and 28.89% of that was discharged to the environment by discharging the hot gases from the exhaust. In the RO subsystem, 0.21% and 0.035% of the total system exergy input were destructed in the membrane and the pump due to the irreversibility, and 0.021% was discharged to the environment because of discharging the exergy by the permeate and brine streams to the environment. By comparing the destructed exergy in the RO subsystem of the GT-RO system (first system) and the GT-VCR-RO system (second system), it can be found that the exergy destruction in the RO subsystem of the GT-VCR-RO system is 33.83% less than that of the GT-RO system. Because the temperature of the RO feed water was increased by recovery of the condenser waste heat, which decreases the energy consumption of the RO pump, consequently increases the total exergy efficiency.

In the VCR subsystem, 0.059% of the total system exergy input was destructed: 0.029%, 0.019%, 0.005%, and 0.006% were destructed in the evaporator, the compressor, the condenser, and the expansion valve, respectively, due to irreversibility of the processes. The irreversibility in the condenser and the evaporator is due to the heat transfer temperature difference between the hot and cold streams.

Tables 11 and 12 list the simulation and exergy analysis results for the  $GT-AC_{H_2O-LiBr}-RO$  system (third system). In Table 12, it

**Table 9**Results of energy thermodynamic simulation for GT-VCR-RO system (second system).

Sub system	Component	State point	Pressure (kPa)	Temperature (°C)	Mass flow rate (kg/s)	Specific enthalpy (kJ/kg)	Energy (kW)	Exergy (Kw)
GT	Com.	1	101	26.43	0.3524	299.94	105.7	0.043
		2	606	244	0.3524	520.71	183.5	73.59
	CC	2	606	244	0.3524	520.51	183.5	73.59
		5	700	35	0.0093	51,428	477.73	506.392
		3	606	1279	0.3614	1698.19	613.7	364
	GT	3	606	1279	0.3614	1698.19	613.7	364
		4	103	1279	0.3614	1113.44	402.4	146.3
VCR	Eva.	11	101	35	0.3524	308.74	108.8	0
		1	101	26.43	0.3524	299.94	105.7	0.043
		12	511.5	16.43	0.0198	106.06	2.1	0
		13	511.5	16.43	0.0198	259.59	5.14	0.0002
	Com.	13	511.5	16.43	0.0198	259.59	5.14	0.0002
		14	976.8	42.02	0.0198	274.24	5.43	0.267
	Con.	14	976.8	42.02	0.0198	274.24	5.43	0.267
		15	976.8	38.5	0.0198	106.06	2.1	0.03
		16	101	25	0.3333	6.21	2.07	0
		6	101	27.39	0.3333	114.85	38.28	-0.1339
	Exp.	15	976.8	38.5	0.0198	106.06	2.1	0.03
		12	511.5	16.43	0.0198	106.06	2.1	0
RO	Pump	6	101	27.39	0.3333	114.85	38.28	-0.1339
	-	7	4266	27.4	0.3333	115.81	38.6	1.218
	Mem.	7	4266	27.4	0.3333	115.81	38.6	1.218
		8	160	27.4	0.1	114.8	11.48	1.125
		9	3642	27.4	0.2333	113.28	26.43	-0.96

can be seen that 69.9% of the total system input exergy was destructed: 69.31% was destructed in the GT power plant subsystem, 0.34% was destructed in the AC $_{\rm H_2O-LiBr}$  subsystem, and 0.25% was destructed in the RO subsystem. In the GT power plant, from the total system exergy input 0.83%, 39.74%, 1.21%, and 0.82% were destructed in the air compressor, the CC, the GT, and the HRSG, respectively, where 26.71% of the input exergy was discharged to the environment by the exhausted hot gasses, which is less than that of the first system. Because some parts of energy in the exhaust gasses were recovered in the HRSG which produces steam as a heat source of the desorber of the AC $_{\rm H_2O-LiBr}$  subsystem.

0.033% and 0.19% of the total system exergy input in the RO subsystem were destructed in the pump and the membrane because of the irreversibility of the pumping process in the pump and the pressure drop through the membrane. Also 0.03% of the total system exergy input was discharged to the environments by permeate and the brine streams. The destructed exergy of the RO

**Table 10**Results of exergy analysis for GT–VCR–RO system (second system).

		Component	Amount (Kw)		Percentage (%)	
Exergy input			506.392		100	
Exergy output			147.87		29.2	
Exergy	GT	Air compressor	4.252	356.9	0.84	70.48
destruction		Combustion	200.1		39.52	
		chamber				
		Gas turbine	6.233		1.23	
		Exhaust	146.3		28.89	
	VCR	Evaporator	0.142	0.296	0.029	0.059
		Compressor	0.097		0.019	
		Condenser	0.027		0.005	
		Expansion value	0.03		0.006	
	RO	RO pump	0.176	1.33	0.035	0.266
		Membrane	1.05		0.21	
		Discharge	0.104		0.021	

subsystem of the GT-VCR-RO and the GT –  $AC_{H_2O-LiB_T}$  – RO systems represents the exergy destruction of the RO part in the GT –  $AC_{H_2O-LiB_T}$  – RO system is less than that of the GT-VCR-RO system. Because the RO feed water temperature of the GT –  $AC_{H_2O-LiB_T}$  – RO system is higher than that of in the GT-VCR-RO system, the pump energy consumption of the third system is more decreased and the exergy destruction is more decreased than the second system.

0.34% of the total system exergy input in the GT - AC $_{\rm H_2O-LiBr}$  - RO system was destructed in the AC $_{\rm H_2O-LiBr}$  subsystem: 0.08%, 0.15%, 0.01%, and 0.06% in the desorber, the absorber, the evaporator, and the condenser, respectively, were destructed due to the irreversibility of the heat transfer in the finite temperature difference and 0.03% was destructed in the expansion valve due to the irreversibility of the expansion process. On the other hand, the exergy destructions of the pump and the SHX were considered negligible.

The exergy analysis results of the three cogeneration systems showed that the system performance can be improved in following four ways: First, the exergy discharged to the environment by the GT exhaust can be recovered as an energy source for other process of the system using an HRSG; therefore, the third cogeneration system  $(GT - AC_{H_2O-LiBr} - RO)$  was suggested to improve the system performance. However, the exergy of the exhaust gas in the third system was not completely recovered in the HRSG since the  $AC_{H_2O-LiBr}$  subsystem was utilized only for cooling the compressor inlet air temperature. Second, the exergy of the discharged streams to the environment in the RO desalination subsystem can be decreased with an ERD (energy recovery device), which uses the brine stream exergy to generate some of the power consumed by the RO pump, which leads to an increase in the exergy efficiency of the system. Third, the components with higher isentropic efficiencies can be used to reduce the exergy destructions in the turbines, compressors, and pumps. Fourth, the reduction of the heat transfer temperature difference between hot and cold streams can reduce the exergy destructions of heat exchangers, e.g., the evaporator, condenser, absorber,

 $\label{eq:Table 11} \textbf{Results of thermodynamic simulation for GT-AC}_{H_2O-LiBr}-\textbf{RO system (third system)}.$ 

Sub system	Component	State point	Pressure (kPa)	Temperature (°C)	Mass flow rate (kg/s)	Specific enthalpy (kJ/kg)	Energy (kW)	Exergy (Kw)
GT	Com.	1	101	14.84	0.3666	288.32	105.7	0.2545
		2	606	224.4	0.3666	500.54	183.5	73.65
	CC	2	606	224.4	0.3666	500.54	183.5	73.65
		5	700	35	0.0098	51,428	506.53	536.92
		3	606	1276	0.3761	1695.29	637.6	377.8
	GT	3	606	1276	0.3761	1695.29	637.6	377.8
		4	103	784.1	0.3761	1111.4	418	151.7
	HRSG	4	103	764.4	0.3761	1111.4	418	151.7
		18	102	653	0.3761	1088.8	409.5	145.4
		19	1100	110	0.004	2562.5	10.25	2.047
		17	1100	110	0.004	440	1.76	0.1635
ABC	Des.	20	1100	110	0.004	2562.5	10.25	1.997
		21	1100	110	0.004	439.25	1.757	0.335
		26	7.445	53.61	0.008	116.25	0.93	0.1693
		27	7.445	100	0.005	262.4	1.312	0.8326
		30	7.445	50.84	0.003	2704.66	8.114	0.5443
	Con.	30	7.445	50.84	0.003	2704.66	8.114	0.5443
	2011	31	7.445	40.16	0.003	175.33	0.526	0.0367
		34	150	25	0.35	105.28	36.85	19.52
		35	150	30.16	0.35	129.97	44.44	19.33
	Exp.	31	7.445	40.16	0.003	175.33	0.526	0.367
	2.10.	32	3.169	25	0.003	175.33	0.526	0.1668
	Eva.	32	3.169	25	0.003	175.33	0.526	0.1668
	Lvu.	33	3.169	25	0.003	2655	7.965	-0.082
		11	101	35	0.3666	308.51	113.1	0
		1	101	14.84	0.3666	288.32	105.7	0.2545
	Abs.	33	3.169	25	0.003	2655	7.965	-0.082
	1103.	24	150	35	0.008	70.875	0.567	0
		29	3.169	79.29	0.005	189	0.945	0.6138
		16	101	25	0.3333	104.86	34.95	0.0130
		6	101	30.98	0.3333	129.88	43.29	-0.2871
	Exp.	28	7.445	58.4	0.005	189	0.945	0.7594
	LAP.	29	3.169	79.29	0.005	189.06	0.9453	0.6138
	Pump	24	3.169	35	0.008	71.125	0.569	0.0130
	rump	25	7.445	35	0.008	71.123	0.6	0.0004
	SHX	25	7.445	35	0.008	75 75	0.6	0.0004
	SIIV	26	7.445 7.445	53.61	0.008	116.25	0.93	0.0004
		26 27	7.445 7.445	100	0.008	262.4		0.1693
		28				262.4 189	1.312	
DO.	December		7.445	58.4	0.005		0.945	0.7594
RO	Pump	6	101	30.98	0.3333	9.87	3.29	-0.2871
	N. 6	7	4225	30.99	0.3333	130.39	43.46	1.045
	Mem.	7	4225	30.99	0.3333	130.39	43.46	1.045
		8	151	30.99	0.1	129.8	12.98	1.157
		9	3917	30.99	0.2333	127.73	29.8	-1.152

 $\label{eq:Table 12} \textbf{Results of exergy analysis for } \textbf{GT-AC}_{\textbf{H}_2\textbf{O-LiBr}}\textbf{-RO system (third system)}.$ 

		Component	Amount (Kw)		Percentage (%)	
Exergy input			536.92		100	
Exergy output			161.61		30.1	
Exergy	GT	Air compressor	4.421	372.14	0.83	69.31
destruction		Combustion chamber	213.4		39.74	
		Gas turbine	6.486		1.21	
		HRSG	4.433		0.82	
		Exhaust	143.4		26.71	
	ABC	Desorber	0.445	1.81	0.08	0.33
		Condenser	0.32		0.06	
		Expansion valves	0.17		0.03	
		Evaporator	0.06		0.01	
		Absorber	0.81		0.15	
		Pump	0.0001		0	
		Solution HX	0.001		0	
	RO	RO pump	0.18	1.36	0.033	0.25
		Membrane	1.04		0.19	
		Discharge	0.137		0.03	

desorber, SHX, and HRSG. However, it is noted that it requires a higher cost of heat exchangers.

### 4. Conclusions

In this study, three cogeneration systems that combined GT power plants and RO desalination systems were optimized based on exergy analysis. The main conclusions drawn from the present study are listed as follows:

- The influences of the compressor inlet air temperature and the fuel-mass flow rate which affect the system exergy efficiency were examined and their optimal conditions were found for the maximum system exergy efficiency of each cogeneration system using a GA.
- 2. Among the three cogeneration systems, the system with AC (GT AC<sub>H2O-LiBr</sub> RO) was determined as the best system with the exergy and the energy efficiencies as well as the net power generation of 30.1%, 31.9%, and 161.6 kW, respectively, which are improved 3.79%, 4.21%, and 38%, compared to the base GT–RO system. Also the cogeneration system with compression refrigeration cycle could increase exergy and

- energy efficiencies as well as net power generation by 2.28%, 3.22%, and 32%, respectively.
- 3. The exergy analysis results showed that the total system exergy input of the GT power plant, the RO system, and the refrigeration system are destructed over 70%, 0.2%, and 0.06%, respectively, where the largest exergy destruction occurs in the combustion process of three cogeneration systems over 39%.

### Acknowledgments

This work was supported by the Korea Science and Engineering Foundation (KOSEF) grant funded by the Korean government (MEST) (KRF-2012-001400) and also by the National Research Foundation of Korea (NRF) grant funded by the Korea government (MSIP) (No. 2008-0061908).

### References

- [1] Bouzayani N, Galanis N, Orfi J. Thermodynamic analysis of combined electric power generation and water desalination plants. Appl Therm Eng 2009;29: 624–33
- [2] Lu YY, Hu YD. Optimum design of reverse osmosis system under different feed concentration and product specification. J Memb Sci 2007;287:219–29.
- [3] Kaghazchi T, Mehri M, Takht Ravanchi M, Kargari A. A mathematical modeling of two industrial seawater desalination plants. Desalination 2010;252:135— 42.
- [4] Janghorban Esfahani I, Ataei A, Shetty KV, Oh TS, Yoo CK. Modeling and genetic algorithm based on multi-objective optimization for the MED-TVC desalination system. Desalination 2012;292:87–104.
- [5] Ataei A, Khalaji Asadi M, Janghorban Esfahani I, Golzari Y, Oh JM. Integration of reverse osmosis and refrigeration systems for energy efficient seawater desalination. Int J Phys Sci 2011;6:2832–43.
- [6] Darwish MA, Al-Fahed S, Charkroum W. A reverse osmosis desalting plant operated by gas turbines. Desalination 2005;173:13–24.
- [7] Popli S, Rodgers P, Eveloy V. Gas turbine efficiency enhancement using water heat powered absorption chillers in the oil and gas industry. Appl Therm Eng 2013;50:918—31.
- [8] Janghorban Esfahani I, Ataei A, Yoo CK. Parametric analysis and optimization of combined gas turbine and reverse osmosis system using refrigeration cycles. Desalin Water Treat 2012;43:149–58.
- [9] Sanaye S, Tahani M. Analysis of gas turbine operating parameters with inlet fogging and wet compression processes. Appl Therm Eng 2012;30:234—44.
- [10] Hosseini R, Beshkani A, Soltani M. Performance improvement of gas turbines of Fars (Iran) combined cycle power plant by intake air cooling using a media evaporative cooler. Energy Convers Manage 2007;48:1055–64.
- [11] Zadpoor AA, Golshan AH. Performance improvement of a gas turbine cycle by using a desiccant-based evaporative cooling system. Energy 2006;31: 2652–64.
- [12] Khaliq A, Dincer I. Energetic and exergetic of a combined heat and power plant with absorption inlet cooling and evaporative aftercooling. Energy 2004;29:2347–58.
- [13] Ehyaei MA, Mozafari A, Alibiglou MH. Exergy, economic and environmental (3E) analysis of inlet fogging for gas turbine power plant. Energy 2011;36: 6851–61.
- [14] Yuan F, Chen Q. A global optimization method for evaporative cooling systems based on entransy theory. Energy 2012;42:181–91.
- [15] Bianco-Marigorta AM, Sanchez-Henriquez MV, Pena-Quinta JA. Exergetic comparison of two different cooling technologies for the power cycle of a thermal power plant. Energy 2011;36:1966–72.
- [16] Sanaye S, Fardad A, Mostakhdemi M. Thermoeconomic optimization of an ice thermal storage systems for gas turbine inlet cooling. Energy 2011;36: 1057–67
- [17] Bilton AM, Wiesman R. On the feasibility of community-scale photovoltaicpowered reverse osmosis desalination systems for remote locations. Renew Energy 2011;36:3246–56.
- [18] Isam HA. Second-low analysis of a reverse osmosis plant in Jordan. Desalination 2009;239:207–15.
- [19] Wang J, Dai Y, Gao L. Exergy analyses and parametric optimizations for different cogeneration power plants in cement industry. Appl Energy 2009:86:941–8.
- [20] Ahmadi P, Dincer I. Thermodynamic and exergoenvironmental analysis, and multi-objective optimization of a gas turbine power plant. Appl Therm Eng 2011;31:2529–40.
- [21] Cerci Y. Exergy analysis of a reverse osmosis desalination plant in California. Desalination 2002;142:257–66.
- [22] Dai Y, Wang J, Gao L. Exergy analysis and optimization for a novel combined power and ejector refrigeration cycle. Appl Therm Eng 2009;29:1983–90.
- [23] Gebreslassie BH, Medrano M, Boer D. Exergy analysis of multi-effect water-LiBr absorption systems: from half to triple effect. Renew Energy 2010;35: 1773–82.

- [24] Sun Z, Wang J, Dai Y, Wang J. Exergy analysis and optimization of a hydrogen production process by a solar-liquefied natural gas hybrid driven transcritical CO<sub>2</sub> power cycle. Int J Hydrogen Energy 2012;37:18731–9.
- [25] Mafi M, Naeynian M, Amidpour M. Exergy analysis of multistage cascade low temperature refrigeration systems used in olefin plants. Int J Refrigeration 2009;32:279–94.
- [26] Ganjeh Kaviri A, Jafar MNM, Lazin TM. Modeling and multi-objective exergy based optimization of a combined cycle power plant using a genetic algorithm. Energy Convers Manage 2012;58:94—103.
- [27] Ahmadi P, Dincer I. Exergoenvironmental analysis and optimization of a cogeneration plant system using multimodel genetic algorithm (GA). Energy 2010;35:5161–72.
- [28] Madlool NA, Saidur R, Rahim NA, Islam MR, Hossian MS. An exergy analysis for cement industries: an overview. Renew Sustain Energy Rev 2012;16: 921–32.
- [29] Tempesti D, Fiaschi D. Thermo-economic assessment of a micro CHP system fuelled by geothermal and solar energy. Energy 2013;58:45–51.
- [30] Tsatsaronis G, Morosuk T. A new approach to the exergy analysis of absorption refrigeration machine. Energy 2008;33:890–907.
- [31] Rezayan O, Behbahaninia A. Thermoeconomic optimization and exergy analysis of CO<sub>2</sub>/NH<sub>3</sub> cascade refrigeration systems. Energy 2006;31:3401–14.
- [32] Fabrega FM, Rossi YS, Angelo YVH. Exergetic analysis of the refrigeration system in ethylene and propylene production process. Energy 2010;35: 1224–31.
- [33] Kilic M, Kaynakli O. Second law-based thermodynamic analysis of water-lithium bromide refrigeration system. Energy 2007;35:1505–12.
- [34] Morosuk T, Tsatsaronis G. Advanced exergetic evaluation of refrigeration machines using different working fluids. Energy 2009;34:2248–58.
- [35] Sharqawy MH, Zubair SM, Lienhard JH. Rebuttal to "Discussion of second law analysis of reverse osmosis desalination plant: an alternative design using pressure retarded osmosis [Energy 2011] 36: 6617–6626]". Energy 2012;46: 691–3.
- [36] Selbas R, Kizilkan O, Sencan A. Thermoeconomic optimization of subcooled and superheated vapor compression refrigeration cycle. Energy 2006;31: 2108–28.
- [37] Salehzadeh A, Khoshbakhtisaray R, Jalalivahid D. Investigating of the effect of several thermodynamic parameters on exergy destruction in components of a tri-generation cycle. Energy 2013;52:96–109.
- [38] Marcovecchio MG, Aguirre PA, Scenna NJ. Global optimal design of reverse osmosis networks for seawater desalination: modeling and algorithm. Desalination 2005;184:259–71.
- [39] Vince F, Marechal F, Aoustin E, Breant P. Multi-objective optimization of RO desalination plants. Desalination 2008;222:96–118.
- [40] Hosseini SR, Amidpour M, Behbahaninia A. Thermoeconomic analysis with reliability consideration of a combined power and multi stage flash desalination plant. Desalination 2011;278:424–33.
- [41] Kurt H, Recebli Z, Gredik E. performance analysis of open cycle gas turbines. Int J Energy Res 2009;33(2):285–94.
- [42] Cetin B. Optimal design of gas turbines. J Dogus Univ 2006;7:59-71.
- [43] Shi X, Che D. Thermodynamic analysis of an LNG fuelled combined cycle power plant with waste heat recovery and utilization system. Int J Energy Res 2007;31:975–98.
- [44] Tozer R, Syed A, Maidment G. Extended temperature—entropy (T–S) diagrams for aqueous bromide absorption refrigeration cycles. Int J Refrigeration 2005;28:689–97.
- [45] Li H, Russell N, Sharifi V, Swithenbank J. Techno-economic feasibility of absorption heat pumps using wastewater as the heating source for desalination. Desalination 2011;281:118–27.
- [46] Huicochea A, Rivera W, Gutierrez-Urueta G, Bruno JC, Coronas A. Ther-modynamic analysis of a trigeneration system considering of a micro gas turbine and a double effect absorption chiller. Appl Therm Eng 2011;31: 3347–53.
- [47] Kaita Y. Thermodynamic properties of lithium bromide-water solutions at high temperatures. Int J Refrigeration 2001;24:374–90.
- [48] Hong D, Tang L, He Y, Chen G. A novel absorption refrigeration cycle. Appl Therm Eng 2010;30:2045–50.
- [49] Yumrutas R, Kunduz M, Kanoglu M. Exergy analysis of vapor compression refrigeration systems. Exergy Int J 2002;2:266–72.
- [50] Dicer I. Environmental and sustainability aspects of hydrogen and fuel cell systems. Int J Energy Res 2007;31:29–55.
- [51] Hosseini SR, Amidpour M, Shakib SE. Cost optimization of combined power and water desalination plant with exergetic, environment and reliability consideration. Desalination 2012;285:123–30.
- [52] Abu Qdais H, Bani Hani K, Shatnawi N. Modeling and optimization of biogas production from a waste digester using artificial neural network and genetic algorithm. Resour Conserv Recycl 2010;54:359–63.
- [53] Elmolla ES, Chaudhuri M, Eltoukhy MM. The use of artificial neural network (ANN) for modeling of COD removal from antibiotic aqueous solution by the Fenton process. J Hazard Mater 2010;179:127–34.
- [54] Sun Y, Zeng WD, Han YF, Ma X, Zhao YQ. Optimization of chemical composition for TC11 titanium alloy based on artificial neural network and genetic algorithm. Comput Mater Sci 2011;50:1064–9.
- [55] Wang J, Yan Z, Wang M, Ma Sh, Dai Y. Thermodynamic analysis and optimization of an (organic Rankin cycle) ORC using low grade heat source. Energy 2013;49:356–65.

- [56] Konak A, Coit DW, Smith AE. Multi-objective optimization using genetic algorithm: a tutorial. Reliab Eng Syst Safety 2006;91:992-1007.
- Saxena NK, Khan A, Pourush PKS, Kumar N. GA optimization of cutoff frequency of magnetically biased microstrip circular patch antenna. Int | Electron
- [58] Liao HC. Using GA to dispatch the obtaining quantity for minimizing the total cost based on consideration of patient safety in HSCM. Expert Syst Appl 2009;36:11358–62.
- [59] Rajendra M, Chandra Jena P, Raheman H. Prediction of optimization pretreatment process parameters for biodiesel production using ANN and GA. Fuel 2009:88:868-75.

### **Nomenclatures**

A: pure water permeability, kg/m<sup>2</sup> s atm

A': baffle parameter

 $A_m$ : membrane area, m<sup>2</sup>

AC: absorption chiller

Abs.: absorber

B: salt permeability, m/s

C: concentration, ppm

CC: combustion chamber

Com.: compressor

Cond.: condenser

Ctd: total drag force

D: salt diffusivity, m<sup>2</sup>/s

Desor.: desorber

 $d_h$ : hydraulic diameter of the feed spacer channel, m

Eva.: evaporator

ET: Expander turbine

Ex: exergy of stream, kW

ex: specific exergy, kJ/kg

FF: fouling factor

G: generator

GT: gas turbine

h: enthalpy

HRSG: heat recovery steam generator

 $h_{\rm sn}$ : height of the feed spacer channel, m

J: flux, kg/m<sup>2</sup> h

 $k_{dc}$ : baffle parameter

*K*<sub>s</sub>: mass transfer coefficient

l: length of filament in the spacer mesh, m

*L*: length of membrane element, m

LHV: Low heat value, kJ/kg

M<sub>s</sub>: molecular weight of solute

mem.: membrane

n: baffle parameter

p: pressure, bar P: pump

 $\Delta P$ : trans-membrane pressure, pa

Q: flow rate, m<sup>3</sup>/h Q: heat rate, kW

r: pressure ratio

Re: Reynolds number

Ref.: refrigeration

RO: reverse osmosis

Ru: universal gasses constant, J/mol K

s: entropy, kJ/kg K Sc: Schmidt number

Sh: Sherwood number

T: temperature, °C
TCF: Temperature correction factor

TMP: trans-membrane pressure

u: velocity, m/s

V<sub>w</sub>: permeation velocity

VCR: vapor-compression refrigeration

W: shaft work

Subscripts

a: air

b: brine

f: feed water

g: flow gas

i: inner

m: membrane

o: outer

p: permeate

ref: refrigerant

s: salt

w: water

### Greek

 $\gamma$ : heat capacity ratio

η: efficiency

 $\varepsilon$ : void fraction of the spacer

μ: viscosity, kg/m s

 $\pi$ : osmotic pressure, bar

 $\rho$ : density, kg/m<sup>3</sup>

 $\omega$ : width of the membrane, m